# Inverse-phase Rabi oscillations in semiconductor microcavities

A. V. Trifonov,[1,*] N. E. Kopteva,[1] M. V. Durnev,[2] I. Ya. Gerlovin,[1] R. V. Cherbunin,[1] A. Tzimis,[3,4] S. I. Tsintzos,[3] Z. Hatzopoulos,[3] P. G. Savvidis,[3,4] and A. V. Kavokin[5,1,6]

[1]*Spin Optics Laboratory, St. Petersburg State University, St. Petersburg 198504, Russia*

[2]*Ioffe Institute, St. Petersburg 194021, Russia*

[3]*Department of Materials Science and Technology, University of Crete, 71003 Heraklion, Crete, Greece*

[4]*FORTH-IESL, P.O. Box 1385, 71110 Heraklion, Crete, Greece*

[5]*School of Physics and Astronomy, University of Southampton, Southampton SO17 1BJ, United Kingdom*

[6]*CNR-SPIN, Viale del Politecnico 1, I-00133, Rome, Italy*

(Received 1 December 2016; revised manuscript received 15 March 2017; published 5 April 2017)

We study experimentally the oscillations of a nonstationary transient signal of a semiconductor microcavity with embedded InGaAs quantum wells. The oscillations occur as a result of quantum beats between the upper and lower polariton modes due to strong exciton-photon coupling in the microcavity sample (Rabi oscillations). The detection of a spectrally resolved signal has allowed for a separate observation of oscillations at the eigenfrequencies of two polariton modes. Surprisingly, the observed oscillations measured at the lower and upper polariton modes have opposite phases. We demonstrate theoretically that opposite-phase oscillations are caused by a pump-induced modification of polariton Hopfield coefficients, which govern the ratio of exciton and photon components in each of the polariton modes. Such behavior is a fundamental feature of the quantum beats of coupled light-matter states. In contrast, the reference pump-probe experiment performed for pure excitonic states in a quantum well heterostructure with no microcavity revealed in-phase oscillations of the pump-probe signals measured at different excitonic levels.

DOI: 10.1103/PhysRevB.95.155304

## I. INTRODUCTION

Microcavity embedded semiconductor nanostructures have been the subject of intense studies during recent years. Due to the high density of the photon field inside a microcavity, these structures feature exceptionally strong light-matter coupling [1]. The effects of strong coupling might be applied for a realization of low-threshold lasers [2,3], logic elements for optical computers [4], memory elements for quantum computations [5,6], sources of terahertz emission [7], etc. Light-matter coupling is most efficient at the resonance between the cavity mode and the exciton transitions inside the cavity. This resonance results in the formation of coupled photon-exciton excitations—exciton-polaritons.

The polariton effect might be observed in various excitonic systems [8], however, it is most pronounced in microcavity structures. In high-finesse microcavities the energy of the exciton-photon interaction is enhanced by about three orders of magnitude as compared to bulk semiconductor materials and thin films. Exciton-photon coupling in microcavities leads to the formation of lower (LP) and upper (UP) polariton modes, which are split by ∼10 meV in typical GaAs-based samples. The excitation of both polariton modes with a short optical pulse leads to the oscillations of exciton polarization and electric field amplitudes at a frequency defined by the value of the splitting between polariton modes (the so-called vacuum Rabi oscillations) [9–17].

The study of Rabi oscillations allows for a detailed understanding of the polariton dynamics in microcavity structures [16–20]. Since the typical values of the Rabi oscillation period lie in a picosecond or subpicosecond range, the most effective way to study Rabi oscillations is to apply the methods of coherent spectroscopy with femtosecond laser pulses. These methods, generally called pump-probe techniques, are based on probing with a probe pulse the changes in the medium properties induced by a pump pulse, and have been used for a long time to study the exciton dynamics in semiconductor nanostructures [21].

The experimental data obtained with the pump-probe technique are usually successfully described by means of optical Bloch equations, where the coupling between the pump and probe pulses is accounted for in the dielectric susceptibility of the structure by the nonlinearity in light amplitude terms [21]. The physical processes responsible for the nonlinearity in semiconductor nanostructures are depletion of the ground state due to a Pauli blockade and the Coulomb screening of excitons, which reduce the oscillator strength of the exciton transition. The depletion of the ground state by a pump field is a common effect for two-level quantum systems, whereas exciton-exciton interactions are typical for semiconductors only.

The dynamics of polaritons in microcavities has much in common with the dynamics of other excitonic systems, however, due to the coupled light-matter nature of the polariton states, there are substantial differences in their behavior. In particular, the introduction of a microcavity results in a significant increase of the photon lifetime inside the sample. As a result, additional effects, such as the blueshift of polariton energy levels under intense optical excitation, appear. As we will show in this paper, it is mainly the blueshift effect that is responsible for the formation of Rabi oscillations in a pump-probe signal.

We have investigated the transient optical response of a semiconductor microcavity with InGaAs quantum wells (QWs) using a spectrally resolved pump-probe technique. We have revealed distinct Rabi oscillations of the optical signals at each of the polariton modes. For all of the excitation conditions

*Corresponding author: arthur.trifonov@gmail.com

 

we tried, the observed oscillations corresponding to the lower and upper polariton modes are found to have opposite phases. In order to identify the nonlinear effects that contribute to the formation of the measured signal, we have developed a theoretical model.

## II. EXPERIMENT

The experimentally studied sample is a relatively low-finesse microcavity ($Q \approx 2000$), which consists of 17 and 21 pairs of AlAs/GaAs layers. The four groups of pairs of $In_xGa_{1-x}As$ quantum wells with different concentrations of In ($x = 0.08$ and $x = 0.12$) are embedded inside the microcavity. The cavity length is variable across the sample plane, which allows one to change the detuning between the exciton and photon modes. The photon mode is tuned to the resonance with a deeper well with $x = 0.12$. The distance between the neighboring QWs is sufficiently large, so that one can neglect the effects of interwell carrier tunneling and coupling. The substrate is transparent in the spectral range of QW excitonic resonance, which allows one to study the sample in the transmission geometry.

The sample was cooled down to a temperature of 5 K in a closed-cycle helium cryostat. In the experimental setup (see Fig. 1), the emission of a femtosecond Ti:sapphire laser with a duration of 100 fs and a repetition frequency of 80 MHz was split into two beams. The first (pump) beam was directed along the sample normal and focused with a lens with a focal length of 150 mm into a spot of 70 $\mu$m diameter. The second (probe) beam was incident at a 5° angle with respect to the sample normal, passing through the delay line and focused into a spot of 30 $\mu$m diameter.

The probe emission passing through the sample was focused into the spectrometer and detected by a nitrogen-cooled CCD camera. The CCD-camera scan was synchronized with a motion of the delay line that allowed us to observe the transmission spectrum as a function of the delay time between the probe and pump pulses.

In the transmission spectrum of the sample [see Fig. 2(a)], two narrow peaks are observed in the range of anticrossing of a polariton dispersion. These two peaks correspond to the upper and lower polariton modes, which are formed in the sample. The investigations were carried out at a sample point with a negative detuning, $\Delta = -3$ meV, between the cavity and exciton modes. The short-period oscillations observed at the spectral contours are related to the light interference in the

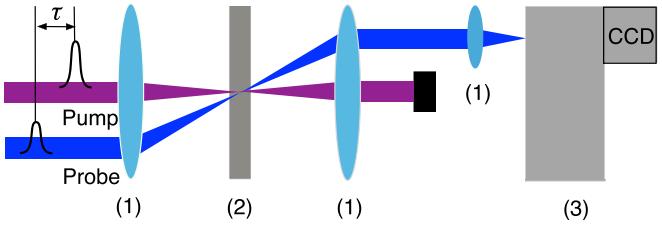


FIG. 1. Schematic sketch of the experimental setup that comprises the lenses (1), the sample (2), and the spectrometer with a CCD camera (3). The probe beam is incident at a 5° angle with respect to the sample normal. The probe pulses are delayed by time $\tau$ with respect to the pump pulse.

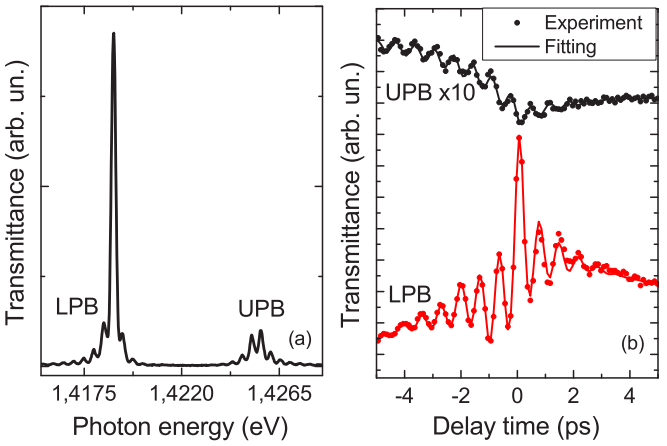


FIG. 2. (a) Transmission spectrum of the studied sample. (b) Intensities of the spectral peaks in the probe transmission spectrum as a function of the delay time between the pump and probe pulses. The black and red dots show the data for the UP and LP frequencies, respectively, and the solid lines are fits (see the text for details). Data for the UP mode are multiplied by a factor of 10. The data are measured at minimal intensities of the pump and probe beams used in the experiment ($P_{pu} = 0.35$ mW and $P_{pr} = 0.1$ mW), which correspond to the polariton density $\lesssim 10^9$ cm$^{-2}$.

sample substrate. With an increase of the excitation power, the LP peak shifts to higher energies, indicating the effects of a polariton-polariton interaction.

The dots in Fig. 2(b) show the dependence of the signal intensity, detected at the UP (black dots) and LP (red dots) modes, as a function of the delay time $\tau$ between the pump and probe pulses. At positive delay time, $\tau > 0$, the pump pulse arrives before the probe one, while $\tau < 0$ corresponds to the first arrival of the probe pulse. The experimental data were approximated with the following phenomenological functions,

$$I^{\pm}_{u,l}(\tau) = \mathcal{F}^{\pm}_{u,l} + \mathcal{A}^{\pm}_{u,l} \exp(\mp\tau/t^{\pm}_{u,l}) + \mathcal{B}^{\pm}_{u,l} \cos(\Omega^{\pm}_{u,l}\tau + \varphi^{\pm}_{u,l}) \exp(\mp\tau/T^{\pm}_{u,l}), \quad (1)$$

where $\mathcal{F}^{\pm}_{u,l}$, $\mathcal{A}^{\pm}_{u,l}$, $\mathcal{B}^{\pm}_{u,l}$, $t^{\pm}_{u,l}$, $T^{\pm}_{u,l}$, $\Omega^{\pm}_{u,l}$, and $\varphi^{\pm}_{u,l}$ are fitting parameters, while the subscripts $u$ and $l$ denote the upper and lower polariton modes, and the superscripts $+$ and $-$ denote the regions of positive and negative $\tau$, respectively. The presented curves are measured at a relatively small pump power, which corresponds to the polariton density $\lesssim 10^9$ cm$^{-2}$. The blueshift of the spectral lines in this case is not resolved.

As seen from Fig. 2, the oscillations of the signal are observed at positive as well as at negative delay times. Moreover, the oscillations at $\tau < 0$ decay slower than at $\tau > 0$, which becomes most pronounced at high pump powers (see Fig. 3). Such an asymmetry of the signal decay is typical for nonlinear optical phenomena driven by third-order nonlinearities [22].

The main result of this work is that the Rabi oscillations observed at the lower and upper polariton modes have an opposite phase (see Fig. 2). This result is valid for all values of pump and probe power used in our experiment. To understand the origin of the inverse-phase oscillations and to specify the nature of the signal at negative delays, we performed a

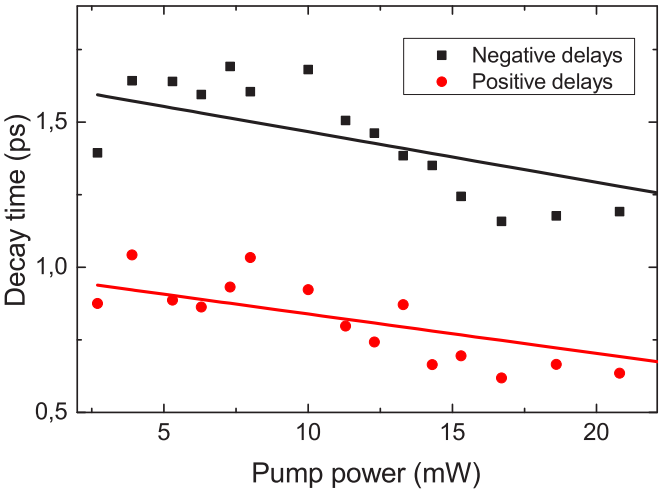


FIG. 3. Oscillation decay time [$T_l^{\pm}$ in Eq. (1)] as a function of pump power at the lower polariton mode. The solid lines are guides for the eye.

theoretical analysis of the polariton dynamics in pump-probe experiments. The results of this analysis are presented in the next section.

## III. THEORY

To analyze the dynamics of the polaritons in our sample we use coupled nonlinear equations which describe the evolution of the photon mode in the microcavity and the exciton polarization in QWs [18,23–25],

$$\frac{\partial P}{\partial t} = [-i(\omega_x - \bar{\omega} + \alpha N_x) - \Gamma]P - i(\Omega_R - \beta N_x)E,$$
$$\frac{\partial E}{\partial t} = [-i(\omega_c - \bar{\omega}) - \gamma]E - i\Omega_R P + \mathcal{E}(t). \quad (2)$$

Here, $E(t)$ is the slowly varying amplitude of the electric field in the center of the QW, $P(t)$ is the slowly varying amplitude of the excitonic polarization averaged over the QW width, $\omega_x$ and $\omega_c$, $\Gamma$ and $\gamma$ are the resonance frequencies and decay rates of the exciton and photon modes, respectively, $\Omega_R$ is the Rabi frequency, which determines the coupling of exciton and photon modes, $\mathcal{E}(t)$ and $\bar{\omega}$ are the amplitude and the optical frequency of the incident electric field, $N_x = |P|^2$ is the exciton population, and $\alpha$ and $\beta$ are real parameters. Equations (2) are analogous to optical Bloch equations that describe four-wave mixing in bulk materials [26].

The incident electric field is a sum of the pump and probe fields inside a cavity, $\mathcal{E} = \mathcal{E}_1 \exp(i\boldsymbol{k}_1\boldsymbol{r}) + \mathcal{E}_2 \exp(i\boldsymbol{k}_2\boldsymbol{r})$, where $\boldsymbol{k}_1$ and $\boldsymbol{k}_2$ are the wave vectors of the pump and probe fields inside the cavity, and $\boldsymbol{r}$ is a coordinate. We model the amplitudes $\mathcal{E}_{1,2}$ to be proportional to delta functions in the time domain $\mathcal{E}_1 = \mathcal{N}_1\delta(t - t_1)$, $\mathcal{E}_2 = \mathcal{N}_2\delta(t - t_2)$, where $\mathcal{N}_1$ and $\mathcal{N}_2$ are the amplitudes, which we assume to be real, and $t_2 - t_1 = \tau$ is the delay time.

Nonlinear terms proportional to $N_x$ enter the first equation in Eqs. (2) and describe two possible nonlinearities in our system. The first one, $\propto \alpha|P|^2P$, is the blueshift of the exciton mode (or the so-called anharmoniclike nonlinearity), and the second one, $\propto \beta|P|^2E$, is the reduction of the Rabi frequency (or the so-called two-level-like nonlinearity) [23,27]. These nonlinear terms result in the coupling of pump and probe signals, and consequently in Rabi oscillations of the output field. The biexcitonic nonlinearity studied in Ref. [23] is neglected in the following.

The electric field and polarization inside the cavity are the sum of the pump and probe components $E = E_1 \exp(i\boldsymbol{k}_1\boldsymbol{r}) + E_2 \exp(i\boldsymbol{k}_2\boldsymbol{r})$ and $P = P_1 \exp(i\boldsymbol{k}_1\boldsymbol{r}) + P_2 \exp(i\boldsymbol{k}_2\boldsymbol{r})$. In the limit of small nonlinearities, $\alpha N_x, \beta N_x \ll \Omega_R$, the approximate solutions of Eqs. (2) have a form

$$E_{1,2} = \bar{E}_{1,2} + \delta E_{1,2}, \quad P_{1,2} = \bar{P}_{1,2} + \delta P_{1,2}, \quad (3)$$

where $\bar{E}_{1,2}$ and $\bar{P}_{1,2}$ satisfy Eqs. (2) at $\alpha = \beta = 0$, and $\delta P_{1,2}$ and $\delta E_{1,2}$ are small corrections due to the presence of nonlinearities.

The time evolution of $\bar{E}_{1,2}$ and $\bar{P}_{1,2}$ is given by [23]

$$\bar{P}_j(t) = -i\mathcal{N}_j \frac{\Omega_R}{\tilde{\Omega}_R} \sin\tilde{\Omega}_R(t - t_j) \times \exp\left[-\frac{\tilde{\gamma} - i\Delta}{2}(t - t_j)\right]\theta(t - t_j),$$
$$\bar{E}_j(t) = \mathcal{N}_j\left[\cos\tilde{\Omega}_R(t - t_j) - i\frac{\Delta}{2\tilde{\Omega}_R}\sin\tilde{\Omega}_R(t - t_j)\right] \times \exp\left[-\frac{\tilde{\gamma} - i\Delta}{2}(t - t_j)\right]\theta(t - t_j). \quad (4)$$

Here, $\tilde{\Omega}_R = \sqrt{\Omega_R^2 + \Delta^2/4}$ and $\Delta = \omega_c - \omega_x$ is the cavity mode detuning, $\tilde{\gamma} = (\gamma + \Gamma)/2$, $\theta(t)$ is a Heaviside function, and we assume $\bar{\omega} = \omega_c$. In the derivation of Eqs. (4) we neglected small terms proportional to $\gamma/\Omega_R \ll 1$ and $\Gamma/\Omega_R \ll 1$.

The nonlinear terms proportional to $\exp(i\boldsymbol{k}_2\boldsymbol{r})$, which give rise to Rabi oscillations in the direction of the probe pulse, are

$$F_{\rm nl} = -i\alpha|P_1|^2P_2 + i\beta(|P_1|^2E_2 + P_1^*P_2E_1). \quad (5)$$

In the experiment we measure the Fourier transform of the output signal in the direction of the probe pulse, which is proportional to

$$I_\omega = |E_{2,\omega}|^2 = |\bar{E}_{2,\omega}|^2 + \bar{E}_{2,\omega}(\delta E_{2,\omega})^* + (\bar{E}_{2,\omega})^*\delta E_{2,\omega}, \quad (6)$$

where $F_\omega$ is the Fourier transform of $F$, $F_\omega = \int F \exp(i\omega t)dt$, and the asterisk means the complex conjugate. In Eq. (6) we neglected a small contribution $|\delta E_{2,\omega}|^2$, which is proportional to the second power of nonlinearities $\alpha$ and $\beta$. Note that the first term in Eq. (6) is a transmission coefficient of the microcavity structure and does not depend on $\tau$.

Solving Eqs. (2) in the frequency space, we find for the Fourier transforms $\bar{E}_{2,w}$ and $\delta E_{2,\omega}$,

$$\bar{E}_{2,w} = i\mathcal{N}_2\frac{\omega + \Delta + i\Gamma}{(\omega + \Delta + i\Gamma)(\omega + i\gamma) - \Omega_R^2},$$
$$\delta E_{2,\omega} = \frac{i\Omega_R F_{{\rm nl},\omega}}{(\omega + \Delta + i\Gamma)(\omega + i\gamma) - \Omega_R^2}, \quad (7)$$

where $F_{{\rm nl},\omega}$ is a Fourier transform of Eq. (5). Using Eqs. (6) and (7) we find for the oscillating transient signal at upper and

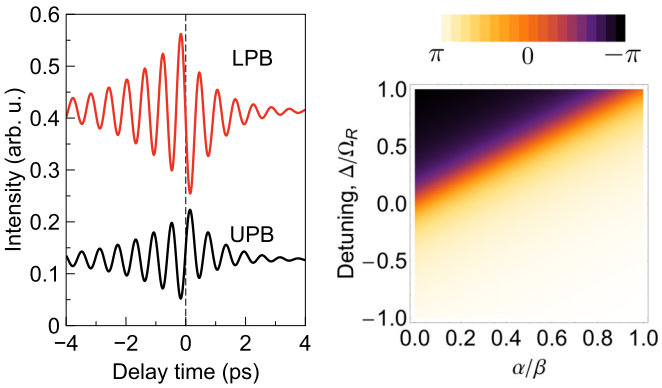


FIG. 4. Left panel: Transient signals calculated using Eqs. (9), (11), and (12). The parameters used are $\Omega_R = 5$ ps$^{-1}$, $\Delta = -3$ ps$^{-1}$, $\gamma = \Gamma = 1$ ps$^{-1}$, and $\alpha/\beta = 5$. Right panel: Phase shift between Rabi oscillations at LP and UP modes at $\tau > 0$. $\Omega_R = 5$ ps$^{-1}$, $\gamma = \Gamma = 1$ ps$^{-1}$.

lower polariton modes,

$$I_{u,l} \equiv I_\omega(\omega_{u,l}) = \frac{2\mathcal{N}_2\Omega_R(\omega_{u,l}+\Delta)}{(2\tilde{\gamma}\omega_{u,l}+\gamma\Delta)^2}\mathrm{Re}\{F_{\mathrm{nl},\omega}(\omega_{u,l})\}, \quad (8)$$

where $\omega_{u,l} \approx -\Delta/2 \pm \tilde{\Omega}_R$ are the real parts of the upper and lower polariton modes under the conditions $\gamma/\Omega_R \ll 1$, $\Gamma/\Omega_R \ll 1$, which are fulfilled in the experiment, and Re denotes the real part of a complex number.

It follows from Eqs. (4), (5), and (8) that the intensities $I^+_{u,l}$ at $\tau > 0$ and $I^-_{u,l}$ at $\tau < 0$ have a form

$$I^\pm_{u,l} = \frac{I_0 e^{-|\tau|/T^\pm}(\omega_{u,l}+\Delta)}{(2\tilde{\gamma}\omega_{u,l}+\gamma\Delta)^2} \times [A^\pm_{u,l} + B^\pm_{u,l}\sin 2\tilde{\Omega}_R\tau + C^\pm_{u,l}\cos 2\tilde{\Omega}_R\tau], \quad (9)$$

where $I_0 = -2\mathcal{N}_1^2\mathcal{N}_2^2\Omega_R^4/\tilde{\Omega}_R^4$. The calculations yield

$$T^+ = 1/\tilde{\gamma}, \quad T^- = 2/\tilde{\gamma}, \quad (10)$$

$$A^+_{u,l} = \frac{1}{8}\left(\alpha + \frac{\pm\tilde{\Omega}_R - \Delta}{\Omega_R}\beta\right), \quad B^+_{u,l} = \frac{\tilde{\Omega}_R}{12\tilde{\gamma}}\left(\alpha - \frac{\Delta}{\Omega_R}\beta\right),$$
$$C^+_{u,l} = -\frac{1}{32}\left(\alpha - \frac{\pm 2\tilde{\Omega}_R + \Delta}{\Omega_R}\beta\right), \quad (11)$$

and

$$A^-_{u,l} = \pm\frac{\beta}{8}, \quad B^-_{u,l} = \frac{\tilde{\Omega}_R}{12\tilde{\gamma}}\left(\alpha - \frac{\Delta}{\Omega_R}\beta\right),$$
$$C^-_{u,l} = \frac{1}{32}\left(3\alpha + \frac{\pm 2\tilde{\Omega}_R - 3\Delta}{\Omega_R}\beta\right). \quad (12)$$

It is noteworthy that the parameters in the phenomenological Eq. (1) are related to the ones in Eq. (9) as $T^\pm_{u,l} = t^\pm_{u,l} = T^\pm$, $\mathcal{A}^\pm_{u,l} \propto A^\pm_{u,l}$, $\mathcal{B}^\pm_{u,l} \propto \sqrt{(B^\pm_{u,l})^2 + (C^\pm_{u,l})^2}$, and $\tan\varphi^\pm_{u,l} = B^\pm_{u,l}/C^\pm_{u,l}$.

With the use of Eqs. (9), (11), and (12) let us now analyze the behavior of Rabi oscillations for the two types of nonlinearities given by Eq. (5) (see Fig. 4). For the anharmoniclike nonlinearity ($\beta = 0$, $\alpha \neq 0$) the intensities at the upper and lower modes $I^\pm_{u,l}$ differ only by the sign of the numerator in Eq. (9), which results in opposite-phase oscillations.

In the case of the two-level-like nonlinearity ($\alpha = 0, \beta \neq 0$) the situation is more complicated. It is seen from Eq. (11) that for $\Delta \neq 0$ the main contribution to $I^\pm_{u,l}$ is given by $B^\pm_{u,l}$, which is parametrically large ($\tilde{\Omega}_R/\tilde{\gamma} \gg 1$). This results again in opposite-phase oscillations. However, if $\Delta = 0$, the coefficient $B^\pm_{u,l}$ vanishes and the oscillations are governed by $C^\pm_{u,l}$, which gives in-phase oscillations.

In general, in-phase oscillations occur in the region of parameters when $B^\pm_{u,l} \ll C^\pm_{u,l}$, i.e., for $\alpha/\beta - \Delta/\Omega_R \ll \tilde{\gamma}/\tilde{\Omega}_R$. Since $\tilde{\gamma}/\tilde{\Omega}_R \ll 1$, this is a very narrow region in the vicinity of $\alpha/\beta = \Delta/\Omega_R$. In the remaining region of the parameters, the phase between the oscillations on the upper and lower modes is equal to $\pm\pi$. We note that in our sample $\Delta < 0$ and therefore, since $\alpha, \beta > 0$, inverse-phase oscillations occur for any ratio between $\alpha$ and $\beta$.

To understand the origin of inverse-phase Rabi oscillations it is also instructive to use a quantum approach based on the secondary quantization of photon and exciton modes and the transition to the polariton basis. The classical values $E$ and $P$ are related to the average values of the exciton and photon field annihilation operators $\hat{\psi}_x$ and $\hat{\psi}_c$ as $P = \langle\hat{\psi}_x\rangle$ and $E = \langle\hat{\psi}_c\rangle$. Both approaches give identical results for the time evolution of $P$ and $E$; the derivation of Eq. (2) starting from the quantum model can be found, e.g., in Ref. [25]. In the strong-coupling regime it is convenient to switch to the polariton basis with the lower- (upper-) branch polariton operators $\hat{\psi}_l = c_1\hat{\psi}_x + c_2\hat{\psi}_c$, $\hat{\psi}_u = c_2\hat{\psi}_x - c_1\hat{\psi}_c$, where $c_{1,2}$ are the Hopfield coefficients [28], which define the photon and exciton contributions at the upper and lower polariton states, and therefore the spectrum of the microcavity transmission coefficient.

We cannot work in the polariton basis using both of the nonlinearities considered in Eq. (5), because the second nonlinearity, which describes the saturation of the oscillator strength, enters only the first equation in the system (2). Indeed, at $\beta \neq 0$ the system matrix is not Hermitian and its eigenvectors are not orthogonal, so the polariton wave functions presented above are not the eigenstates of the system under study. Hence we limit our consideration to the case of $\alpha \neq 0$, $\beta = 0$. In the limit of small nonlinearity, $\alpha N_x \ll \Omega_R$, the straightforward calculations yield

$$|c_1|^2 = |c_1(0)|^2 - \frac{2\alpha\Omega_R^2}{\left(\Delta^2 + 4\Omega_R^2\right)^{3/2}}N_x,$$
$$|c_2|^2 = |c_2(0)|^2 + \frac{2\alpha\Omega_R^2}{\left(\Delta^2 + 4\Omega_R^2\right)^{3/2}}N_x, \quad (13)$$

where $|c_{1,2}(0)|^2 = (1 \pm \Delta/\sqrt{\Delta^2 + 4\Omega_R^2})/2$ are the Hopfield coefficients at $N_x = 0$. The coefficients $c_1$ and $c_2$ describe the photon contribution to the upper and lower polariton states, respectively, and therefore Eqs. (13) give information about the microcavity transmission coefficient at the corresponding frequencies. Due to the constraint $|c_1|^2 + |c_2|^2 = 1$ [and as seen from Eqs. (13)], any change in $|c_1|^2$ induced by nonlinearity results in an opposite change of $|c_2|^2$, leading to opposite-phase Rabi oscillations of the transient signal.

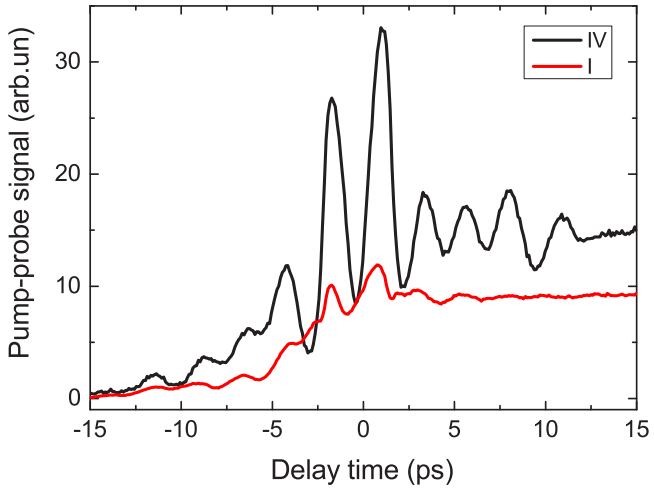


FIG. 5. Pump-probe signals of quantum beats between the I and IV quantum-confined excitonic states in the 95 nm InGaAs/GaAs quantum well. The signals were measured by tuning the detected photon energy at the I and IV excitonic resonances. The frequency of the signal oscillations corresponds to the energy splitting between these states.

## IV. DISCUSSION

The opposite-phase signal in the region of positive delays (the standard pump-probe signal) is governed by a nonlinearity of the type $(P_1 P_1^*)P_2$, corresponding to the scattering of the probe pulse on the excitonic polarization created by the pump pulse. In the region of negative delays, the oscillating signal (the four-wave mixing signal) is governed by the nonlinearity $(P_2 P_1^*)P_1$, which has the same mathematical form, however, in that case it corresponds to the scattering of the pump pulse on the polarization pattern created by the simultaneous action of the pump and probe pulses. Such an asymmetry should result in a twofold increase of the signal decay time at $\tau < 0$ $(T^+)$ compared to $\tau > 0$ $(T^-)$, as confirmed by Eq. (10). Such behavior is observed in experiments in a wide range of pump powers for the LP mode and at low pump powers for the UP mode (see Fig. 3). The increase of the $T^-/T^+$ ratio at higher pump powers for UP mode might be attributed to exciton-exciton scattering, which drives the phase relaxation of polarization.

To confirm that the inverse-phase behavior of Rabi oscillations is a specific feature of microcavity systems with strong light-matter coupling, we performed the same experiment for a quantum well structure without Bragg mirrors. We investigated the sample with an InGaAs quantum well of 95 nm width and 2% indium concentration. In the absorption and photoluminescence spectra we observed a series of narrow lines corresponding to optical transitions to or from the quantum-confined excitonic levels. Detailed characteristics of the sample and experimental details can be found in Refs. [29,30].

Figure 5 shows the intensities of the pump-probe signals measured at energies corresponding to the transitions to the first and fourth quantum-confined levels. The energy difference between the levels is approximately 2 meV, which is comparable to the Rabi splitting in the microcavity sample. One can see distinct signal oscillations, caused by quantum beats between the excitonic states. In contrast to the microcavity sample, the oscillation phases at the two energies coincide, which is typical for quantum beats between matter excitations, such as excitons [31]. Indeed, for excitonic quantum beats the microscopic mechanism of the pump-probe signal is related mainly to the depopulation of the ground state due to pump beam excitation [32]. In this case the quantum beats observed at optical transitions into two excited states have equal phases.

## V. CONCLUSION

To conclude, we studied a transient pump-probe signal through a microcavity heterostructure with an embedded InGaAs quantum well. The studies revealed well-pronounced oscillations related to the quantum beats between the lower and upper polariton modes (vacuum Rabi oscillations). The principal result is that the observed oscillations measured at the lower and upper polariton levels have opposite phase. As revealed by the theoretical analysis, the opposite phases of the oscillations are related to the specific light-matter character of the polariton states in the microcavity, in contrast to quantum beats between pure matter excitations. The experiments showed that, in agreement with theoretical predictions, the oscillations in the region of positive delay time between the pump and probe pulses decay twice faster than in the region of negative delay time.

## ACKNOWLEDGMENTS

Financial support from the SPbU (Grant No. 11.38.277.2014), the RFBR, and DFG in the frame of International Collaborative Research Center TRR 160 (Project No. 15-52-12018) is acknowledged. A.V.T. and R.V.C. are thankful to the RFBR for financial support in the frame of Grant No. 15-59-30406-PT. M.V.D. was partially supported by RFBR Project No. 16-32-60175, the Russian Federation President Grant No. MK-7389.2016.2, and the Dynasty Foundation. A.K. acknowledges partial support from the HORIZON 2020 RISE project CoExAn (Grant No. 644076). The authors thank the SPbU Resource Center "Nanophotonics" (photon.spbu.ru) for providing the sample with a wide quantum well studied in this work.

[1] C. Weisbuch, M. Nishioka, A. Ishikawa, and Y. Arakawa, Phys. Rev. Lett. **69**, 3314 (1992).

[2] C. Schneider, A. Rahimi-Iman, N. Y. Kim, J. Fischer, I. G. Savenko, M. Amthor, M. Lermer, A. Wolf, L. Worschech, V. D. Kulakovskii *et al.*, Nature (London) **497**, 348 (2013).

[3] P. Bhattacharya, B. Xiao, A. Das, S. Bhowmick, and J. Heo, Phys. Rev. Lett. **110**, 206403 (2013).

[4] D. Ballarini, M. De Giorgi, E. Cancellieri, R. Houdré, E. Giacobino, R. Cingolani, A. Bramati, G. Gigli, and D. Sanvitto, Nat. Commun. **4**, 1778 (2013).

[5] C. Leyder, T. C. H. Liew, A. V. Kavokin, I. A. Shelykh, M. Romanelli, J. P. Karr, E. Giacobino, and A. Bramati, Phys. Rev. Lett. **99**, 196402 (2007).
[6] S. S. Demirchyan, I. Y. Chestnov, A. P. Alodjants, M. M. Glazov, and A. V. Kavokin, Phys. Rev. Lett. **112**, 196403 (2014).
[7] T. C. H. Liew, M. M. Glazov, K. V. Kavokin, I. A. Shelykh, M. A. Kaliteevski, and A. V. Kavokin, Phys. Rev. Lett. **110**, 047402 (2013).
[8] V. A. Kiselev, B. S. Razbirin, and I. N. Ural'tser, JETP Lett. **18**, 296 (1973).
[9] T. B. Norris, J.-K. Rhee, C.-Y. Sung, Y. Arakawa, M. Nishioka, and C. Weisbuch, Phys. Rev. B **50**, 14663 (1994).
[10] P. V. Kelkar, V. G. Kozlov, A. V. Nurmikko, C.-C. Chu, J. Han, and R. L. Gunshor, Phys. Rev. B **56**, 7564 (1997).
[11] G. Bogiovanni, A. Mura, F. Quochi, S. Gürtler, J. L. Staehli, F. Tassone, R. P. Stanley, U. Oesterle, and R. Houdré, Phys. Rev. B **55**, 7084 (1997).
[12] M. Shirane, C. Ramkumar, Y. P. Svirko, H. Suzuura, S. Inouye, R. Shimano, T. Someya, H. Sakaki, and M. Kuwata-Gonokami, Phys. Rev. B **58**, 7978 (1998).
[13] A. Brunetti, M. Vladimirova, D. Scalbert, M. Nawrocki, A. V. Kavokin, I. A. Shelykh, and J. Bloch, Phys. Rev. B **74**, 241101 (2006).
[14] T. C. H. Liew, Y. G. Rubo, and A. V. Kavokin, Phys. Rev. B **90**, 245309 (2014).
[15] M. De Giorgi, D. Ballarini, P. Cazzato, G. Deligeorgis, S. I. Tsintzos, Z. Hatzopoulos, P. G. Savvidis, G. Gigli, F. P. Laussy, and D. Sanvitto, Phys. Rev. Lett. **112**, 113602 (2014).
[16] L. Dominici, D. Colas, S. Donati, J. P. Restrepo Cuartas, M. De Giorgi, D. Ballarini, G. Guirales, J. C. López Carreño, A. Bramati, G. Gigli, E. del Valle, F. P. Laussy, and D. Sanvitto, Phys. Rev. Lett. **113**, 226401 (2014).
[17] D. Colas, L. Dominici, S. Donati, A. A. Pervishko, T. C. H. Liew, I. A. Shelykh, D. Ballarini, M. De Giorgi, A. Bramati, G. Gigli *et al.*, Light: Sci. Appl. **4**, e350 (2015).
[18] N. Takemura, M. D. Anderson, S. Trebaol, S. Biswas, D. Y. Oberli, M. T. Portella-Oberli, and B. Deveaud, Phys. Rev. B **92**, 235305 (2015).
[19] N. Takemura, M. D. Anderson, S. Biswas, M. Navadeh-Toupchi, D. Y. Oberli, M. T. Portella-Oberli, and B. Deveaud, Phys. Rev. B **94**, 195301 (2016).
[20] N. Takemura, S. Trebaol, M. D. Anderson, V. Kohnle, Y. Léger, D. Y. Oberli, M. T. Portella-Oberli, and B. Deveaud, Phys. Rev. B **92**, 125415 (2015).
[21] J. Shah, *Ultrafast Spectroscopy of Semiconductors and Semiconductor Nanostructures*, 2nd ed. (Springer, Berlin, 1999).
[22] E. L. Ivchenko, *Optical Spectroscopy of Semiconductor Nanostructures* (Alpha Science, Harrow, U.K., 2005).
[23] Y. Fu, M. Willander, E. L. Ivchenko, and A. A. Kiselev, Phys. Rev. B **55**, 9872 (1997).
[24] G. Rochat, C. Ciuti, V. Savona, C. Piermarocchi, A. Quattropani, and P. Schwendimann, Phys. Rev. B **61**, 13856 (2000).
[25] H. Carmichael, *An Open Systems Approach to Quantum Optics* (Springer, Berlin, 1993).
[26] We note that to describe the evolution of the excitonic mode, the so-called excitonic Bloch equations were used in recent works [18,24]. In this approach there is a third equation, which accounts for additional decay channels of exciton population $N_x$ as compared to polarization decay $\Gamma$. The inclusion of these addition channels does not change the general conclusions of our work, therefore we neglect them and use $N_x = |P|^2$.
[27] S. Schmitt-Rink, S. Mukamel, K. Leo, J. Shah, and D. S. Chemla, Phys. Rev. A **44**, 2124 (1991).
[28] J. J. Hopfield, Phys. Rev. **112**, 1555 (1958).
[29] A. V. Trifonov, S. N. Korotan, A. S. Kurdyubov, I. Y. Gerlovin, I. V. Ignatiev, Y. P. Efimov, S. A. Eliseev, V. V. Petrov, Y. K. Dolgikh, V. V. Ovsyankin, and A. V. Kavokin, Phys. Rev. B **91**, 115307 (2015).
[30] A. V. Trifonov, I. Y. Gerlovin, I. V. Ignatiev, I. A. Yugova, R. V. Cherbunin, Y. P. Efimov, S. A. Eliseev, V. V. Petrov, V. A. Lovtcius, and A. V. Kavokin, Phys. Rev. B **92**, 201301 (2015).
[31] P. Gilliot, D. Brinkmann, J. Kudrna, O. Crégut, R. Lévy, A. Arnoult, J. Cibert, and S. Tatarenko, Phys. Rev. B **60**, 5797 (1999).
[32] M. Mitsunaga and C. L. Tang, Phys. Rev. A **35**, 1720 (1987).